0026-895X/11/7904-681–691$20.00
MOLECULAR PHARMACOLOGY
Vol. 79, No. 4
68031/3675362
Mol Pharmacol 79:681–691, 2011
Printed in U.S.A.

Why Does the Inner-Helix Mutation A413C Double the Stoichiometry of Kv1.3 Channel Block by Emopamil but Not by Verapamil?

Alexey Rossokhin, Tobias Dreker, Stephan Grissmer, and Boris S. Zhorov

Department of Biochemistry and Biomedical Sciences, McMaster University, Hamilton, Ontario, Canada (A.R., B.S.Z.); Research Centre of Neurology, Russian Academy of Medical Sciences, Moscow (A.R.); Sechenov Institute of Evolutionary Physiology and Biochemistry, Russian Academy of Sciences, St. Petersburg, Russia (B.S.Z.); 4SC AG, Planegg-Martinsried, Germany (T.D.); and Institute of Applied Physiology, Ulm University, Ulm, Germany (S.G.)

Received August 5, 2010; accepted January 10, 2011

ABSTRACT

hKv1.3 channels in lymphocytes are targets for the chemotherapy treatment of autoimmune diseases. Phenylalkylamines block Kv1.3 channels by poorly understood mechanisms. In the inactivation-reduced mutant H399T, the second mutation A413C in S6 substantially decreases the potency of phenylalkylamines with a *para*-methoxy group at the phenylethylamine end, whereas potency of phenylalkylamines lacking this group is less affected. Intriguingly, completely demethoxylated emopamil blocks mutant H399T/A413C with a 2:1 stoichiometry. Here, we generated a triple mutant, H399T/C412A/A413C, and found that its emopamil-binding properties are similar to those of the double mutant. These data rule out disulfide bonding Cys412–Cys413, which would substantially deform the inner helix, suggest a clash of Cys413 with the *para*-methoxy group, and provide a distance constraint to dock phenylalkylamines in a Kv1.2-based homology model. Monte Carlo minimizations predict that the verapamil ammonium group donates an H-bond to the backbone carbonyl of Thr391 at the P-loop turn, the pentanenitrilephenyl moiety occludes the pore, whereas the phenylethylamine *meta*- and *para*-methoxy substituents approach, respectively, the side chains of Met390 and Ala413. In the double-mutant model, the Cys413 side chains accept H-bonds from two emopamil molecules whose phenyl rings fit in the hydrophobic intersubunit interfaces, whereas the pentanenitrilephenyl moieties occlude the pore. Because these interfaces are unattractive for a methoxylated phenyl ring, the ammonium group of respective phenylalkylamines cannot approach the Cys413 side chain and binds at the focus of P-helices, whereas the *para*-methoxy group clashes with Cys413. Our study proposes an atomistic mechanism of Kv1.3 block by phenylalkylamines and highlights the intra- and intersubunit interfaces as ligand binding loci.

Introduction

Potassium channels play fundamental roles in physiology (Hille, 2001), being targets for chemotherapy of cardiovascular, neurological, autoimmune, and other disorders (Chandy et al., 2004; Tamargo et al., 2004; Wulff and Zhorov, 2008). Kv1.3 channels are involved in the activation of T lymphocytes and therefore play an important role in the immune activity (Chandy et al., 1984; DeCoursey et al., 1984). Verapamil, which belongs to the class of phenylalkylamines, blocks Kv1.3 channels with low micromolar concentration (Jacobs and DeCoursey, 1990; DeCoursey, 1995; Rauer and Grissmer, 1996, 1999; Dreker and Grissmer, 2005). Verapamil was originally identified as an antagonist of L-type calcium channels in the heart and vascular smooth muscles (Wit and Cranefield, 1974; Pelzer et al., 1982). Later, verapamil was found to block potassium channels in neurons (Kostyuk et al., 1975), lymphocytes (DeCoursey et al., 1985) and other tissues. Phenylalkylamines have a flexible alkylamine chain flanked by aromatic rings A and B that are proximal, respectively, to the isopropyl and amino groups in the chain (Fig. 1). The amino group of verapamil is predominantly protonated at physiological pH (Retzinger et al., 1986). A permanently charged derivative of verapamil, *N*-methyl-verapamil, acts from the intracellular but not the extracellular side, and the channel opening is required for the drug to reach its binding site (DeCoursey, 1995; Rauer

This work was supported by the Natural Sciences and Engineering Research Council of Canada; and the Deutsche Forschungsgemeinschaft (Martinsried, Germany) [Grants 848/141 and 4SC AG].

Computations were made possible by the facilities of the Shared Hierarchical Academic Research Computing Network (SHARCNET, http://www.sharcnet.ca).

A.R. and T.D. contributed equally to the study. S.G. and B.S.Z. should be considered co-senior authors.

Article, publication date, and citation information can be found at http://molpharm.aspetjournals.org.

doi:10.1124/mol.110.068031.

ABBREVIATIONS: MCM, Monte Carlo energy minimization.

and Grissmer, 1996; Zhang et al., 1999). The rate of the K^+ current block by the externally applied verapamil increases with the external pH (DeCoursey, 1995; Zhang et al., 1999), indicating that verapamil crosses the lipid membrane in the deprotonated form and reaches the receptor from the cytoplasm.

Block of Kv1.3 by externally applied phenylalkylamines resembles state-dependent block of the squid potassium channels by internally applied quaternary ammonium compounds (DeCoursey, 1995), which are known to block the intracellular vestibule of potassium channels (Armstrong, 1971; Armstrong and Hille, 1972). Compounds that block Kv1.3 at the extracellular vestibule such as kaliotoxin, charybdotoxin, and extracellular tetraethylammonium do not compete with verapamil in the blocking of K^+ current (Rauer and Grissmer, 1996, 1999). However, internal application of the *N*-methyl-verapamil or tetraethylammonium in combination with verapamil revealed competition for the channel block (Rauer and Grissmer, 1996, 1999). Thus, several lines of evidence suggest that verapamil and internally applied quaternary ammonium drugs have overlapping binding sites in the inner pore region.

Kv1.3 is formed by four identical subunits. Each subunit contains six membrane-spanning segments and a membrane re-entering P-loop. The pore region is formed by the outer (S5) and inner (S6) helices connected by the P-loop. The latter includes the pore helix (P), the ascending limb with the signature-sequence VGYG whose backbone carbonyls line the selectivity filter, and the extracellular linker between the ascending limb and S6. In the X-ray structures of bacterial and mammal potassium channels (Doyle et al., 1998; Jiang et al., 2002; Long et al., 2005), several interfaces between the pore-forming α-helical segments are seen. S6s from neighboring subunits line four interfaces. In homology models of sodium and calcium channels, corresponding interfaces between domains III and IV contain residues whose mutations affect access and binding of different ligands (Zhorov and Tikhonov, 2004; Bruhova et al., 2008; Tikhonov and Zhorov, 2008; Cheng et al., 2009). Extracellularly applied permanently charged compounds, which cannot permeate the membrane, were proposed to reach their binding sites within the inner pore through the III/IV domain interface (Tikhonov et al., 2006; Bruhova et al., 2008; Tikhonov and Zhorov, 2008). Some ligands of the Kv1.5 channel were also proposed to reach their binding site via the intersubunit interface (Strutz-Seebohm et al., 2007). Because the experimental evidences for the existence of such a pathway in Kv channels are limited, we use the term "niche" to indicate that the interface is reachable for certain moieties of some ligands from the inner pore (Wulff and Zhorov, 2008). Besides the intersubunit niches, potassium channels have intrasubunit niches lined by S6 and P helices. Although the intrasubunit niches are rather narrow in the X-ray structures, they contain ligand-sensing residues. Thus, mutation $M^{p47}I$ (see Fig. 2A for residue labels) decreases the tetraethylammonium potency more than 50-fold (Choi et al., 1993).

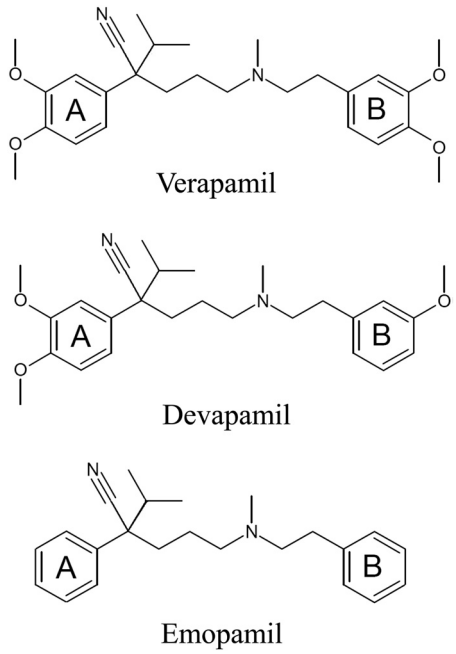

Fig. 1. Structural formulae of verapamil, devapamil, and emopamil.

Dreker and Grissmer (2005) found that in the background of the $H^{p56}T$ mutation with the reduced slow inactivation, the second mutation $A^{i11}C$ substantially decreases potency of verapamil and other phenylalkylamines with a *para*-methoxy group in ring B, whereas the potencies of phenylalkylamines lacking this group are less sensitive to the mutation (Dreker and Grissmer, 2005). Intriguingly, among several tested phenylalkylamines, only emopamil and only in the $A^{i11}C$ mutant demonstrates the Hill coefficient of 2 for the channel block (Dreker and Grissmer, 2005). The rationale for these observations is unclear. For example, the bulky side chain of C^{i11} can sterically obstruct the ligand binding. Besides, because the hydrophobicity index of cysteine is similar to that of valine (Nagano et al., 1999), the SH group of C^{i11} would make the phenylalkylamine receptor more hydrophobic. On the other hand, the proximity of the engineered C^{i11} and the native C^{i10} suggests that the side chains of these two residues could be linked by a disulfide bond. Such a bond would deform the inner helix that lines the inner pore, in which phenylalkylamines ligands are expected to bind.

To explore whether the mutation $A^{i11}C$ affects phenylalkylamine block as a result of local changes at the upper third of the inner helix or because of the inner pore deformation upon possible C^{i10}–C^{i11} disulfide bonding, we generated here a triple mutant $H^{p56}T/C^{i10}A/A^{i11}C$ and demonstrated that its emopamil-binding properties are similar to those of the double mutant $H^{p56}T/A^{i11}C$. These data strongly suggest that the effect of mutation $A^{i11}C$ on the ligand binding is due to direct interaction of the engineered cysteine with the ligands. Furthermore, the fact that phenylalkylamines with the *para*-methoxy group in ring B are most sensitive to the $A^{i11}C$ mutation suggests that the *para*-methoxy group approaches the A^{i11} side chain in the wild-type channel, thus providing an important distance constraint to dock verapamil and other phenylalkylamines. To elaborate a structural interpretation of the experimental data, we have built homology models of the open-state channel and its mutants and used Monte Carlo energy minimizations to optimize the geometry of the channels and dock verapamil and emopamil. Our calculations predicted that in the channel with the native residue A^{i11}, the ammonium group of verapamil would donate an H-bond to the backbone carbonyl of T^{p48} at the C-end of P-helix, the bulky pentanenitrilephenyl moiety would bind in

the inner pore extending toward the cytoplasm, whereas ring B would enter the intrasubunit niche between the S6 and P helices with *para*- and *meta*-methoxy groups approaching, respectively, the side chains of A^{i11} and M^{p47}. In the model with the engineered C^{i11}, the latter obstructed the entrance to the intrasubunit niche from the inner pore. Verapamil in this channel model adopted another binding mode with the ammonium group at the focus of P-helices and the *para*-methoxy group in ring B approaching C^{i11}. Our modeling further predicted that emopamil can form an H-bond N-H---S with the cysteine, extend its ring B in the intersubunit niche, and expose ring A with the isopropyl group to the central cavity. Two emopamil molecules could easily bind in such modes. The hydrophobic intersubunit niche seems too small and unattractive for the methoxylated ring B of verapamil or devapamil (Fig. 1), an analog of verapamil that exhibits the highest Kv1.3-blocking potency among phenylalkylamines tested by Dreker and Grissmer (2005). Our study rationalizes the structure-activity of phenylalkylamines in Kv1.3 and highlights the role of inter- and intrasubunit niches as ligand-binding loci.

Materials and Methods

Designation of Residues and Mutants. In this study, we designate residues using a universal labeling scheme (Zhorov and Tikhonov, 2004), which is described in Fig. 2A. Because the universal scheme needs explanations, we used traditional residue numbers in this article's title and Abstract. Relations between the residue labels and numbers are shown in Fig. 2A. A mutant is designated using a

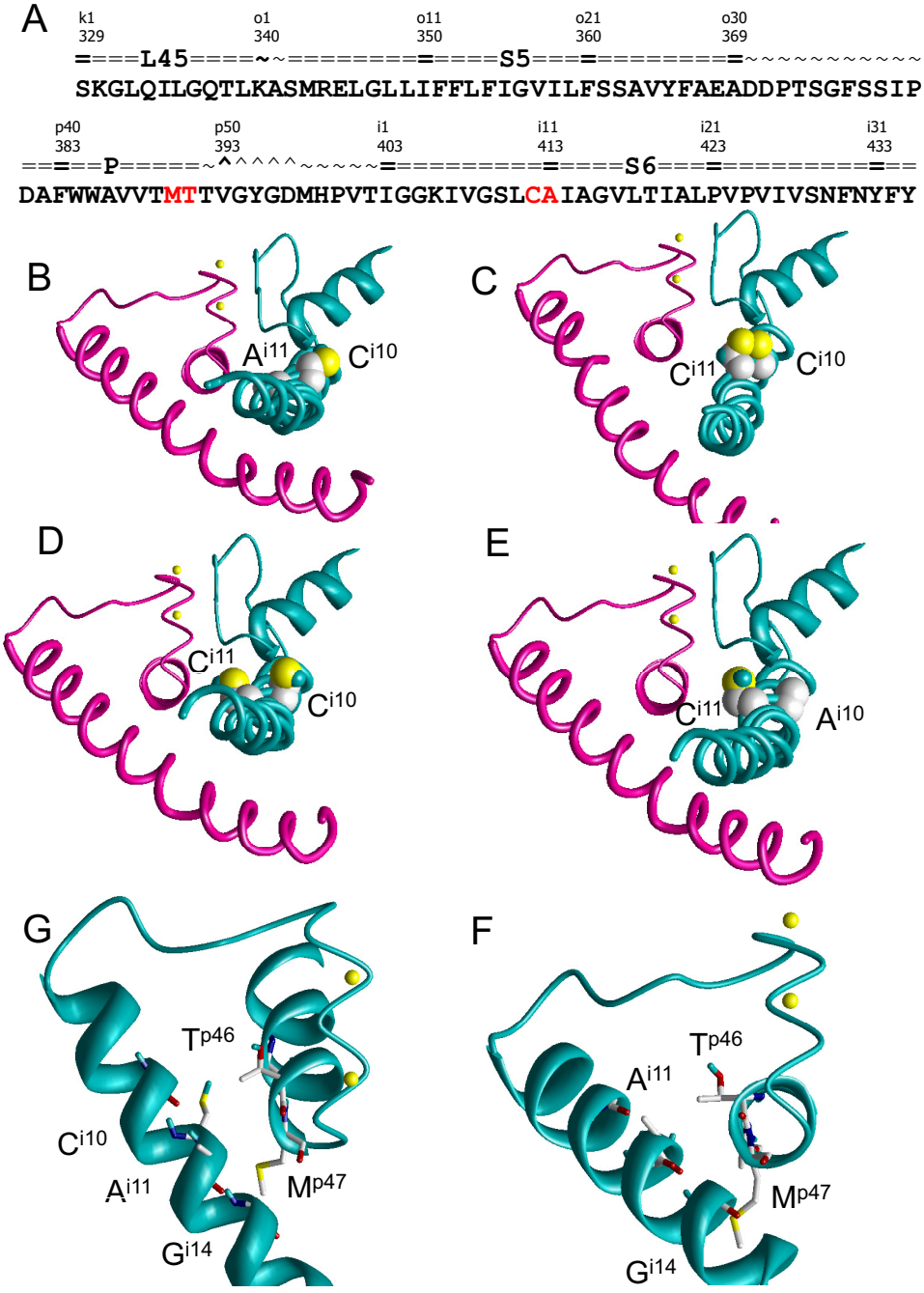

Fig. 2. Inter- and intrasubunit interfaces in the Kv1.3 channel and its mutants. A, human Kv1.3 pore domain sequence. Special symbols mark helices (=), loops/turns (~), and the selectivity-filter region (^). Residue labels and numbers are shown above the respective residues. A label consists of a segment-encoding character and the relative number of the residue in the segment. Character *k* stands for a linker L45, *o* for an outer helix (S5), *p* for a P-loop, and *i* for an inner helix (S6). B to E, intersubunit interface in the homology model of the wild-type Kv1.3, which contains the dipeptide fragment C^{i10}-A^{i11} (B), in the mutant $A^{i11}C$ without (D) and with (C) disulfide bond between the adjacent cysteines C^{i10}–C^{i11}, and in the triple mutant $C^{i10}A/A^{i11}C$, which contains the dipeptide fragment A^{i10}–C^{i11} (E). The models are viewed along the pore helix of magenta-colored subunit. Only S6s and the P-loops in two neighboring subunits are shown for clarity. Cysteine residues are space-filled. Note the different dimensions of the space between two S6s and the P-loop. The tiny yellow balls are potassium ions in sites 1 and 3. F and G, intrasubunit interface between the S6 and P-helices in the X-ray structure of the Kv1.2 channel with the residues in the interface shown as sticks. F, side view. G, view from inside the pore, along the P-helix. The S6 side of the interface has C^{i10}, A^{i11}, and G^{i14}. The P-helix side contains T^{p46} and M^{p47}. The entrance to the interface from the inner pore is guarded by small A^{i11} and the flexible side chain M^{p47}. The tiny yellow balls are potassium ions in sites 1 and 3.

one-letter code for the amino acid in the wild-type channel, its substitution in the mutant channel, and the position label as a superscript between the encoded amino acids.

Cells. The COS 7 cell line was obtained from the Deutsche Sammlung von Mikroorganismen und Zellkulturen GmbH (Brauschweig, Germany). Cells were maintained in Dulbecco's modified Eagle's medium with high glucose (Invitrogen, Carlsbad, CA) containing 10% fetal calf serum (PAA Laboratories GmbH, Pasching, Austria) and cultured at 37°C and 5% pCO_2.

Chemicals and Solutions. All measurements were performed in an extracellular bath solution containing 160 mM NaCl, 2 mM $CaCl_2$, 1 mM $MgCl_2$, 4.5 mM KCl, and 5 mM HEPES, with an osmolarity of 290 to 320 mOsm and pH adjusted to 7.4 with NaOH. The intracellular pipette solution contained 155 mM KF, 2 mM $MgCl_2$, 10 mM EGTA, and 10 mM HEPES with an osmolarity of 290 to 320 mOsM and pH adjusted to 7.2 with KOH. Emopamil (a generous gift from Prof. Dr. Hans-Günther Knaus and Prof. Dr. Hartmut Glossmann, Institut für Biochemische Pharmakologie, Medizinische Universität Innsbruck, Austria) was dissolved in dimethyl sulfoxide as stock solution and diluted to the final concentration in the extracellular bath solution before application. The dimethyl sulfoxide fraction in the final solution was always <2%.

Electrophysiology. The whole-cell recording mode of the patch-clamp technique (Hamill et al., 1981) was used throughout all measurements. Drug effects were evaluated by the steady-state current block obtained during 200-ms voltage steps from −80 to +40 mV every 30 s at room temperature (18–22°C). Electrodes were pulled from glass capillaries (Science Products, Hofheim, Germany) in three stages and fire-polished to resistances of 2 to 4 MΩ. Data were acquired with an EPC-9 patch-clamp amplifier (HEKA Elektronik, Lambrecht/Pfalz, Germany) connected to a personal computer running Pulse/PulseFit version 8.47 data acquisition and analysis software. All currents were filtered by a 2.9-kHz Bessel filter and recorded with a sampling frequency of 2.00 kHz. Capacitative and leak currents were subtracted.

Molecular Biology. The hKv1.3 mutant channels were generated by introducing point mutations in the hKv1.3 wild-type gene contained in a pRc/CMV plasmid vector (a generous gift from Prof. Dr. O. Pongs, Institut für Neurale Signalverarbeitung, Zentrum für Molekulare Neurobiologie, Hamburg, Germany) and confirmed by sequencing. Expression of the mutant genes in COS7 cells was accomplished by cotransfection of ~1 μg of plasmid DNA and ~0.5 μg of eGFP-N1 DNA (Clontech, Mountain View, CA) using FuGENE 6 (Roche Molecular Biochemicals, Indianapolis, IN) as transfection reagent. One day after transfection, sufficient protein levels for electrophysiological measurements were obtained.

Energy Calculations. Available X-ray structures of K^+ channels show a different number of K^+ ions in the selectivity filter: two in the KcsA-antibody complex at low K^+ concentration (Doyle et al., 1998; Zhou et al., 2001a), three in KcsA (Doyle et al., 1998), and four in KvAP (Jiang et al., 2003), in the KcsA-antibody at high K^+ concentration (Zhou et al., 2001a), in KcsA blocked by tetrabutylammonium (Zhou et al., 2001b), and in Kv1.2 (Long et al., 2005). We numbered the sites for K^+ in the selectivity filter from 1 to 4 starting from the most extracellular site. Only two K^+ ions reside in the selectivity filter simultaneously, suggesting K^+ oscillation between positions 1/3 and 2/4 (Morais-Cabral et al., 2001; Zhou and MacKinnon, 2003). We have shown previously that *d*-tubocurarine interacts most preferably with the model in which K^+ ions occupy sites 1 and 3 (Rossokhin et al., 2006). In this study, we used the same configuration.

The Monte Carlo energy minimization (MCM) method (Li and Scheraga, 1987) was used to optimize the Kv1.3 model and to dock the drugs. Energy was minimized in the space of generalized (internal) coordinates using the ZMM program (Zhorov, 1981) (http://www.zmmsoft.com). The generalized coordinates included torsional angles of the channel and ligands, bond angles of ligands, Cartesian coordinates of ions, and variables that govern rigid-body positions and orientations of ligands, water molecules, and the channel subunits. Nonbonded interactions were calculated using the AMBER force field (Weiner et al., 1984, 1986), with a cutoff distance of 9 Å. Electrostatic interactions and solvation energy were calculated with solvent exposure- and distance-dependent dielectric function (Garden and Zhorov, 2010). Because the protonation state of ionizable residues and location of counterions for ionized residues are unknown, we considered all ionizable residues in their neutral forms (Momany et al., 1975; Lazaridis and Karplus, 1999). The atomic charges of the protonated (*R*)-verapamil and (*R*)-emopamil were calculated by AM1 method (Dewar et al., 1985) using program MOPAC (http://openmopac.net/). Bond angles at all heavy atoms of the ligands were allowed to vary during energy minimization.

Homology Models. In this study, we did not address the effect of mutation $H^{p56}T$, which retards C-type inactivation, on the P-domain geometry. Because low micromolar concentrations of verapamil block the wild-type Kv1.3 (Rauer and Grissmer, 1996) and its $H^{p56}T$ mutant (Dreker and Grissmer, 2005), this mutation is unlikely to affect dramatically the drug binding region. Therefore, all calculations were performed using homology models with the wild-type residue H^{p56}. The X-ray structure of Kv1.2 in the open state (Long et al., 2005) was used as template to build homology models of the wild-type Kv1.3 and its mutant. The $A^{i11}C$ mutant was calculated with and without the disulfide bond between C^{i10} and C^{i11}. The models were intensively MC-minimized using the advantage of the 4-fold symmetry of the channel, which has been found highly efficient in constraints-driven large-scale modifications of the *Shaker* channel models (Bruhova and Zhorov, 2005). In calculations with the 4-fold symmetry, the pore axis coincided with the *z*-axis of the Cartesian coordinate system. Torsional angles were sampled in only one subunit (called a parent subunit) and images of the remaining three subunits arranged symmetrically around the pore axis were generated. During MC minimizations, any change of a torsional angle in the parent subunit caused identical changes of the same torsional angle in the three images. Intrasubunit interactions were calculated only within the parent subunit, but all intersubunit interactions and interactions of each subunit with potassium ions and water molecules were considered. The symmetric models were optimized in two stages. At the first stage, pin constraints were used to preserve the channel folding that could be distorted by strong repulsions between side chains in the homology model. (A pin is a penalty function that allows a penalty-free deviation of the respective atom up to 1 Å from the template and imposes an energy penalty for larger deviations.) After the first round of MC-minimizations, all constraints were removed and the model was refined in the second MCM trajectory. In both stages, MC-minimizations were terminated when the last 2000 energy minimizations did not improve the energy of the apparent global minimum.

Ligand Docking. The advantage of the channel symmetry cannot be used for docking of asymmetric ligands. This docking was performed with the channel torsions sampled independently in the four subunits. Unbiased docking of highly flexible ligands such as phenylalkylamines in flexible proteins remains a challenge for methodology of global minimization and for force fields, which should ensure a match between the global minimum of the free energy and the experimental structure. In view of these challenges, we did not attempt an unbiased large-scale search for the lowest-energy binding modes but used experimental data to bias the location of certain phenylalkylamine moieties in potential ligand-binding loci and optimized the constraint-imposed binding poses by MC minimizations. It is noteworthy that after finding the lowest-energy conformation in a constrained MCM trajectory, all constraints were removed and another MCM search for the lowest energy complex was performed. If the unconstrained trajectory caused a noticeable displacement of the ligand from the constraint-imposed binding mode, the corresponding binding mode was disregarded. Each docking experiment involved three MCM trajectories. At the first trajectory, the targeted position of the ligand was imposed by a distance constraint with specific

residues, backbone torsions, and ligand bond angles kept rigid, whereas the ligand position, orientation, conformation, and protein side chain conformations were optimized. At the second trajectory, 10 lowest energy structures found in the first trajectory were MC-minimized with all degrees of freedom (including those governing positions and orientation of potassium ions and water molecules) allowed to vary. At the third trajectory, all drug-channel constraints were removed, and the 10 lowest energy complexes found in the second trajectory were MC-minimized.

Results

Disulfide Bonding Bent S6s in the $A^{i11}C$ Mutant Model. The point mutation $A^{i11}C$ dramatically decreases the channel-blocking potency of verapamil and other phenylalkylamines with the methoxylated ring B (Dreker and Grissmer, 2005). Two explanations for this observation can be proposed. First, the bulky engineered cysteine at the interface between the P-helix and the S6 helix may hinder binding of a phenylalkylamine moiety in the intra- or intersubunit niche. Second, the point mutation may cause nonlocal conformational changes of the channel protein. A point mutation normally is not expected to substantially change the backbone geometry. However, sequentially adjacent cysteines may form disulfide bonds (Zhang and Snyder, 1989) that would distort the backbone. To estimate possible distortions, we MC-minimized three models: the wild-type Kv1.3 channel, the $A^{i11}C$ mutant with the disulfide bonds C^{i10}–C^{i11} in all four subunits, and the $A^{i11}C$ mutant without the disulfide bonds. In the model with the disulfide bonds, the subunit interface viewed along the P-helix is substantially wider than in the wild-type channel (Fig. 2, B and C). In this model, S6 helices were substantially deformed. These deformations can be easily explained by the fact that the distance between β carbons of the adjacent disulfide-bonded cysteines C^{i10} and C^{i11} (4.07 Å) is 1.17 Å smaller than in the $A^{i11}C$ mutant model without the disulfide bonds (5.24 Å). Such a substantial decrease of the distance between β-carbons can be achieved only because of deformation of backbone torsions. These torsional deformations should shift parts of the α-helix on both sides of the disulfide bridge. Compared with the wild-type channel model (Fig. 2B), only the C-terminal parts of S6s in the disulfide-bonded model shifted substantially. A shift of the N-terminal third of S6 was opposed by a knob-into-hole contact between G^{i3} and valine in the AVY motif at the C-end of S5. In the $A^{i11}C$ mutant model without the disulfide bonds, the inner helices only minimally rearranged versus the wild-type Kv1.3 model (Fig. 2, B and D).

The widened hydrophobic interface between neighboring S6 helices in the $A^{i11}C$ mutant might accommodate a part of the ligand and thus explain binding of two emopamil molecules to the channel. However, it is unknown whether C^{i10} and C^{i11} are engaged in the disulfide bond. To address this question, we have generated a triple mutant and explored the stoichiometry of emopamil binding as described below. Our rationale for a triple mutant instead of a different double mutant is that phenylalkylamines bind to the channel with A^{i11} much stronger than to the channel with C^{i11}. Introducing another mutation at this position would result in a strong binding, a weak binding, or something in between. This would not really help in testing the hypothesis on the disulfide bond formation.

Similar Electrophysiological Properties of $H^{p56}T$, $H^{p56}T/A^{i11}C$, and $H^{p56}T/C^{i10}A/A^{i11}C$ Channels. To explore whether the newly generated triple-mutant channel ($H^{p56}T/C^{i10}A/A^{i11}C$) of hKv1.3 has a dramatically altered behavior, we performed a detailed characterization of the electrophysiological properties of the triple mutant channel and compared these properties with those for the single ($H^{p56}T$) and double ($H^{p56}T/A^{i11}C$) mutant channels. The comparison is shown in Fig. 3 for the voltage-dependence of activation (Fig. 3, A, C, and E) and for the use-dependence of inactivation (Fig. 3, B, D, and F). The current traces of the double and triple mutant look very similar, indicating that these channels did not dramatically differ from each other. A summary of the intrinsic properties of the hKv1.3 wild-type and mutant channels is further shown in Table 1.

Similar Block of $H^{p56}T/A^{i11}C$ and $H^{p56}T/C^{i10}A/A^{i11}C$ Channels by Emopamil. To explore whether the mutation $A^{i11}C$ affects ligand action directly or indirectly, via the formation of the disulfide bonding between C^{i10} and C^{i11}, we compared the emopamil stoichiometry in the double and triple mutants. We reasoned that if the Hill coefficient of emopamil binding in the $A^{i11}C$ mutant increases because of S6 deformations caused by the disulfide bonding, the disulfide-

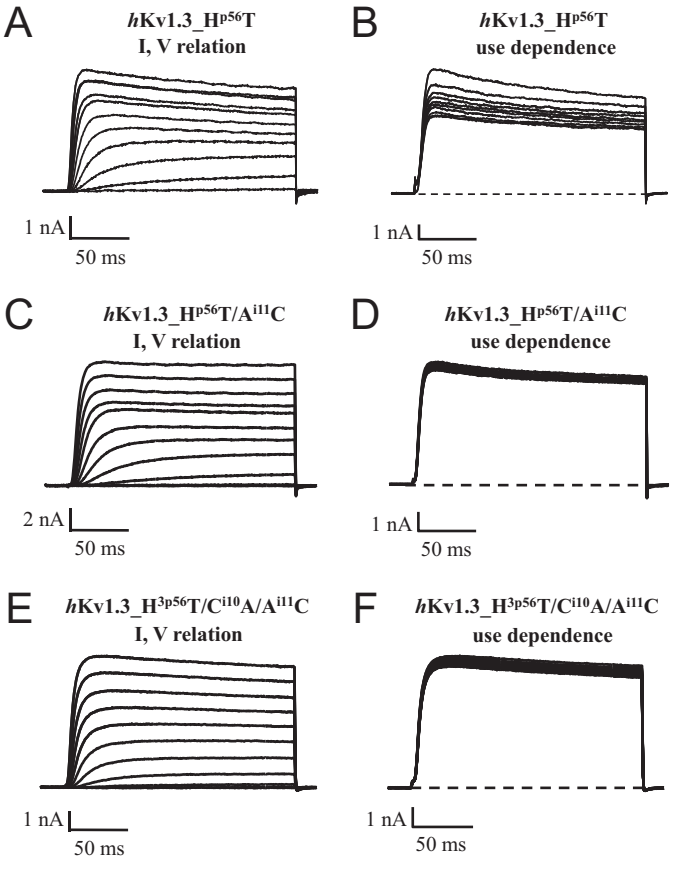

Fig. 3. Currents through single ($H^{p56}T$), double ($H^{p56}T/A^{i11}C$), and triple ($H^{p46}T/C^{i10}A/A^{i11}C$) mutant hKv1.3 channels. A, C, and E. I/V relationship of currents through single (A), double (C), and triple (E) mutant hKv1.3 channels. The displayed currents were induced by consecutive 200-ms voltage pulses from the holding potential of −80 mV to potentials ranging from −50 to +50 mV with an increment of 10 mV for each pulse. B, D, and F: use-dependence of currents through single (B), double (D), and triple (F) mutant hKv1.3 channels. The displayed currents were induced by 10 consecutive 200-ms voltage pulses from the holding potential of −80 to +40 mV every second.

bond elimination in the triple mutant would restore the 1:1 emopamil stoichiometry as in the C-type inactivation reduced hKv1.3_H^{p56}T channels that we explored before (Dreker and Grissmer, 2005). Figure 4A shows steady-state K^+ currents through single-mutant hKv1.3_H^{p56}T channels in the absence (control) and presence of 20 μM emopamil. Emopamil (20 μM) resulted in a steady-state block of current through hKv1.3_H^{p56}T channels at the end of the 200-ms pulse to less than 10% of the control current. This directly reflects the ratio of hKv1.3_H^{p56}T channels in the open and open-blocked state. Using different emopamil concentrations, we have generated a dose-response curve for emopamil to block steady-state currents at the end of a 200-ms depolarizing voltage step (Fig. 4B) as published previously (Dreker and Grissmer, 2005). A fit to the data (solid line) indicated that one emopamil molecule binds reversibly to one mutant channel (Hill coefficient close to 1), thereby preventing current flow with an IC_{50} value for emopamil to block steady-state current of the mutant hKv1.3_H^{p56}T channel of 2 μM. The double mutant hKv1.3_H^{p56}T/A^{i11}C channel is much less sensitive to block by emopamil, as can be seen in Fig. 5A. Emopamil (20 μM) resulted in a steady-state block of current through the double mutant hKv1.3_H^{p56}T/A^{i11}C channels at the end of the 200-ms pulse to ~80% of the control current. Similar results have been obtained previously (Dreker and Grissmer, 2005). In addition, emopamil blocked current through the double mutant hKv1.3_H^{p56}T/A^{i11}C channel with a 2:1 stoichiometry, as can be seen in the dose-response curve shown in Fig. 6.

To test whether possible disulfide bonds between C^{i10} and C^{i11} contribute to the observed changes in affinity and stoichiometry of emopamil block in the double mutant, we generated a triple-mutant hKv1.3_H^{p56}T/C^{i10}A/A^{i11}C channel and investigated the effects of emopamil on current through this triple mutant channel. The results are shown in Fig. 5B. Application of 20 μM emopamil resulted in a steady-state block of current through the triple mutant hKv1.3_H^{p56}T/C^{i10}A/A^{i11}C channels at the end of the 200-ms pulse to ~80%

TABLE 1

Intrinsic properties of the hKv1.3 wild-type channel and the single (H^{p56}T), double (H^{p56}T/A^{i11}C), and triple (H^{p56}T/C^{i10}A/A^{i11}C) mutant channels transiently transfected in COS7 cells

All values are given as mean ± S.D.; numbers of independent experiments are given in parentheses. Values for the wild-type, the single-mutant, and the double-mutant channels are from Dreker and Grissmer (2005).

Properties	Wild Type	H^{p56}T	H^{p56}T/A^{i11}C	H^{p56}T/C^{i10}A/A^{i11}C
$V_{1/2}$, mV	−33 ± 1 (2)	−36 ± 1 (9)	−37 ± 1 (3)	−10 ± 3 (4)
K, mV	10 ± 1 (2)	7 ± 1 (9)	7 ± 1 (3)	11 ± 1 (4)
τ_m, ms	2.9 ± 0.4 (6)	3.9 ± 0.7 (10)	4.9 ± 1.1 (10)	4.5 ± 1.2 (4)
τ_h at +40 mV, ms	291 ± 53 (6)	678 ± 134 (10)	1220 ± 200 (10)	1943 ± 1300 (4)
τ_t at −60 mV, ms	117 (1)	434 ± 119 (8)	30 ± 14 (9)	32 ± 2 (2)
τ_{rec} at −120 mV, s	13.6 ± 0.2 (4)	≤ 1.1 (4)	≤ 1.1 (4)	N.D.

N.D., not determined.

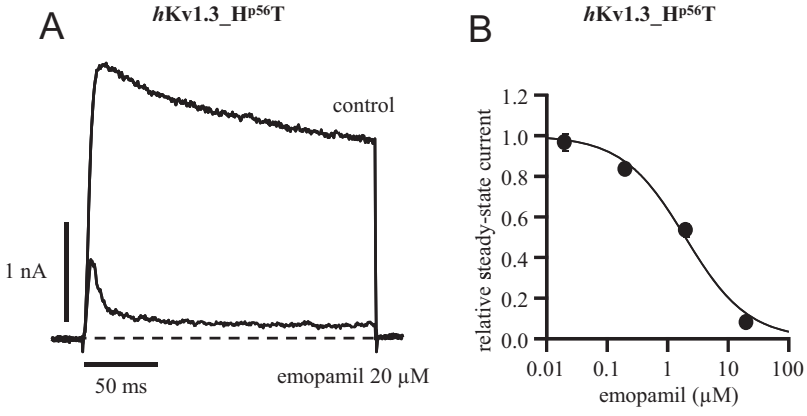

Fig. 4. Effect of extracellularly applied emopamil on steady-state current through mutant hKv1.3_H^{p56}T channels. A, currents were elicited by 200-ms depolarizing voltage steps from a holding potential of −80 to 40 mV every 30 s in the absence (control) and presence of 20 μM emopamil. Shown are steady-state currents in the two solutions. B, dose-response curve for emopamil block of steady-state currents through hKv1.3_H^{p56}T mutant channels. Curve-fitting resulted in an IC_{50} value of 2.0 μM and a Hill coefficient of 0.8 (data from Dreker and Grissmer, 2005).

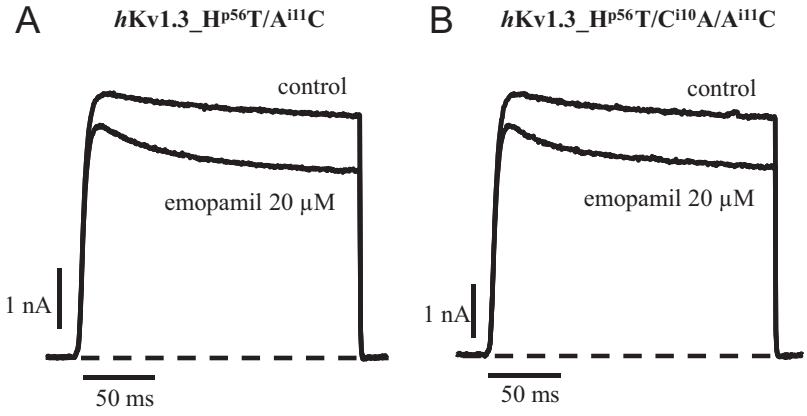

Fig. 5. Effect of extracellularly applied emopamil on steady-state current through the double (A; H^{p56}T/A^{i11}C) and the triple (B; H^{p56}T/C^{i10}A/A^{i11}C) mutant hKv1.3 channels. Currents were elicited by 200-ms depolarizing voltage steps from a holding potential of −80 to +40 mV every 30 s in the absence (control) and presence of 20 μM emopamil. Shown are steady-state currents in the two solutions.

of the control current. This result is almost identical with the results obtained for the effect of emopamil on the double mutant hKv1.3_$H^{p56}T/A^{i11}C$ channel. Likewise, the stoichiometry for emopamil to block current through the triple mutant channel (dose-response curve in Fig. 6) is almost identical with that for the double mutant channel.

Docking of Verapamil and Emopamil in the Wild-Type Kv1.3 and $A^{i11}C$ Mutant. The above experimental data ruled out a possibility that mutation $A^{i11}C$ decreases the potency of phenylalkylamines with the *para*-methoxy group in ring B and increases stoichiometry of the channel block by emopamil through distortion of the inner helices because formation of a disulfide bond C^{i10}–C^{i11}. The alternative hypothesis is that the mutation $A^{i11}C$ decreases potency of verapamil and other phenylalkylamines with the *para*-methoxy group in ring B because the latter clashes with the bulky side chain of the engineered cysteine C^{i11}. This hypothesis provides an important distance constraint to dock verapamil in the wild-type and mutated channels.

We used a distance constraint to impose the *para*-oxygen in ring B of verapamil to be within 6 Å from the β-carbon of A^{i11}. Such a large distance was chosen to impose no specific contacts but just to bring the *para*-oxygen in proximity of A^{i11}. MC minimization of the complex in the presence of the constraint, and then the refinement MC minimization without constraints, predicted two low-energy binding modes. In the lowest-energy model (Fig. 7, A–D), the ammonium group donated an H-bond to the backbone carbonyl of T^{p48}. This carbonyl at the P-loop turn does not accept an H-bond from the upstream backbone amides and therefore constitutes an attractive acceptor for an H-bond from the ligand. In this binding mode, a large part of ring B entered the intrasubunit niche with the *meta*- and *para*-methoxy groups approaching the side chains of M^{p47} and A^{i11}, respectively (Fig. 7C).

In the second-best model in terms of ligand-channel energy, the ammonium group of verapamil occurred at the focus of the P-helices, the *meta*-methoxy groups approached the intrasubunit niche between S6 and the P-helix, and the *para*-methoxy group entered the intersubunit niche between two inner helices and approached the methyl group of A^{i11} without establishing strong contacts with it (Fig. 7F). The verapamil-channel energy in this model is ~1.6 kcal/mol higher (less favorable) than in the first model, but this difference is not large enough to choose one of the models based on energetics only. The second binding mode is consistent with the data that *N*-methyl-verapamil blocks Kv1.3 with the potency similar to that of verapamil (Rauer and Grissmer, 1996). Indeed, the focus of the P-helices is rather far from any residue of the channel and would easily accommodate the quaternary ammonium group of *N*-methyl-verapamil, which cannot donate an H-bond. This fact, however, does not rule out a possibility that verapamil donates an H-bond to the backbone carbonyl of T^{p48} as shown in Fig. 7, B and C, because similar potencies of verapamil and *N*-methyl-verapamil may result from two binding modes shown in Fig. 7, which have many common features. The advantage of the first model is the penetration of ring B in the intrasubunit niche and therefore a closer proximity of the *meta*-methoxy group in ring B to M^{p47}. This methionine in position *p47* is proposed to contribute to the verapamil binding site because the mutation $M^{p47}V$ decreases verapamil potency (Rauer and Grissmer, 1999). MC minimization of verapamil in the $A^{i11}C$ mutant channel from the starting points that correspond to both binding modes shown in Fig. 7 yielded structures with weaker channel-ligand energy because the bulky side chain of cysteine C^{i11} clashed with the *para*-methoxy group (data not shown).

Binding of two emopamil molecules in the modes shown in Fig. 7 is not possible because the focus of the P-helices cannot accommodate two ammonium groups. MC minimization of Kv1.3 with two emopamil molecules from the starting point shown in Fig. 7, A and C, yielded a model with the ammonium groups of two emopamil molecules donating H-bonds to two carbonyls of T^{p48}, but the ligand-channel energies for each ligand were significantly higher (weaker interactions) than that for verapamil because the inner pore is not large enough to accommodate two pentanenitrilephenyl moieties from two ligands.

Intensive MC minimization of Kv1.3 with a single emopamil resulted in a complex in which the ligand ammonium group donated an H-bond to the sulfur atom of C^{i11}. Such binding mode is possible only when the ring B of the ligand deeply penetrates in the intersubunit niche. The channel easily accommodated two emopamil molecules bound in such a mode (Fig. 8, A and B), whereas pentanenitrilephenyl moieties of the two ligands established favorable hydrophobic contacts with each other (Fig. 8C). It is noteworthy that all residues around the hydrophobic phenyl ring B of emopamil are hydrophobic (Fig. 8*D*). Furthermore, ring B fits tightly in the intersubunit niche, whereas the *para*- and/or *meta*-methoxy substituents would sterically clash with the bulky hydrophobic residues there. These features of the model shown in Fig. 8 readily explain why emopamil but not phenylalkylamines with the methoxylated ring B block Kv1.3 with the 2:1 stoichiometry.

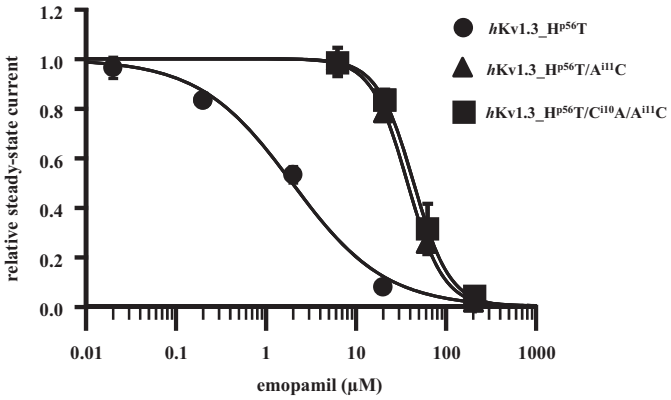

Fig. 6. Dose-response curve for emopamil block of steady-state currents through the double (blue, $H^{p56}T/A^{i11}C$) and the triple (red, $H^{p56}T/C^{i10}A/A^{i11}C$) mutant hKv1.3 channels. Data points at each concentration are from at least two independent measurements. Curve-fitting resulted in an IC_{50} value of 36 μM with a Hill coefficient of 2.2 for the double mutant hKv1.3_$H^{p56}T/A^{i11}C$ channel and an IC_{50} value of 42 μM with a Hill coefficient of 2.2 for the triple mutant hKv1.3_$H^{p56}T/C^{i10}A/A^{i11}C$ channel, respectively. The dose-response curve for emopamil block of steady-state currents through hKv1.3_$H^{p56}T$ mutant channels (from Fig. 3B) is included in this graph for comparison.

Discussion

Phenylalkylamines constitute a promising class of blockers of the medicinally important Kv1.3 channels. Previous studies revealed interesting structure-activity relationships of

phenylalkylamines in the C-type inactivation-reduced mutant hKv1.3_H^{p56}T and the double mutant hKv1.3_H^{p56}T/A^{i11}C. The most challenging paradox is the different stoichiometry of the channel block by verapamil and devapamil on one hand and demethoxylated emopamil on the other hand. Previously proposed qualitative rationale for this paradox (Dreker and Grissmer, 2005) lacks atomistic details. Our initial attempts to elaborate these details by means of molecular modeling suggested different mechanistic explanations for the experimental data: 1) the substantial deformation of the inner helices as a result of possible disulfide bonding between native C^{i10} and engineered C^{i11}; and/or 2) the direct interactions of phenylalkylamines with the side chain of C^{i11}. To choose between these mechanisms, we generated here a triple mutant *h*Kv1.3_H^{p56}T/C^{i10}A/A^{i11}C, in which disulfide bonding between the neighboring inner helix residues is impossible, and therefore substantial deformations of the inner helices are unlikely. The fact that stoichiometry and other characteristics of emopamil action in the triple mutant occurred similar to those in the double mutant ruled out the first mechanism and allowed us to focus on the second mechanism.

The unbiased predictive docking of flexible ligands in proteins remains a challenge even when using a simplified computational approach, when a protein is treated as a rigid body. This methodology cannot guarantee that an apparent global minimum found in energy calculations corresponds to the experimental structure found by the X-ray crystallography (Garden and Zhorov, 2010). Expectations that the real structure of a ligand-channel complex would correspond to an

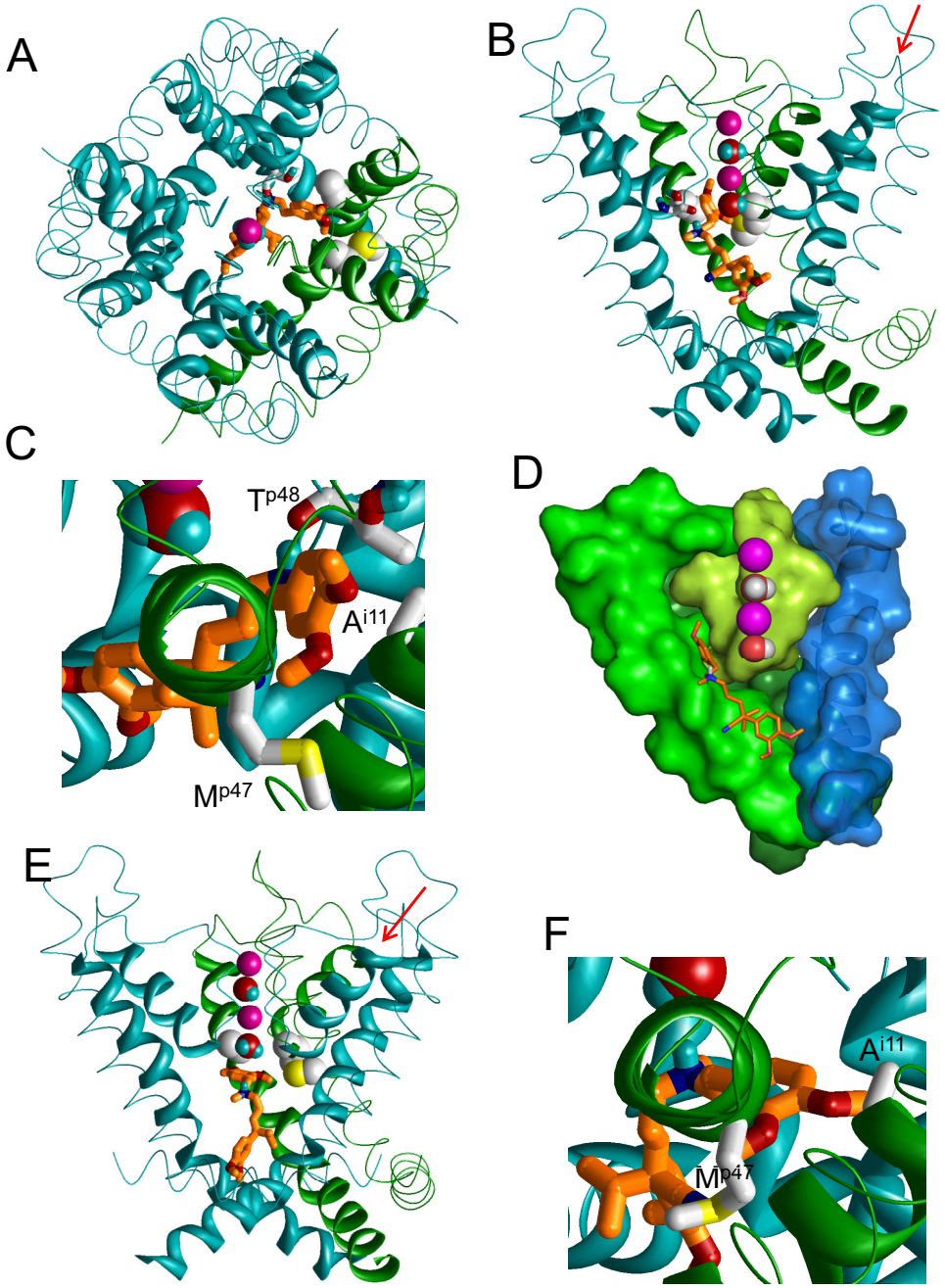

Fig. 7. Verapamil binding in the inner pore of Kv1.3. Shown are extracellular (A), side (B, D, and E), and close-up (C and F) views at predicted binding modes along the red arrows in B and E, respectively. For clarity, one subunit is removed in B and E and two subunits are removed in D. In all, except for D, the P-helices and the inner helices are shown as smooth helices, the outer helices and the L45 linkers as strands, the ascending limbs in the outer pore, and the extracellular linkers as rods. Three subunits are colored cyan and one subunit is colored green. K^+ ions, water molecules, and the side chains of M^{p47} and A^{i11} (A, B, and E) are space-filled. A to D, The first binding mode in which verapamil (orange carbons) donates an H-bond to the backbone carbonyl of T^{p48} (C), whereas ring B extend into the intrasubunit niche. The latter is seen in the surface representation (D) in which S5, P-loop, and S6 of one subunit are dark green, yellow-green, and light green, respectively, and S6 of the neighboring subunit is cyan. E and F, in the second binding mode the ammonium group of verapamil is located at the focus of the P-helices. In both binding modes, the *p*-methoxy group in ring B approaches the methyl group of A^{i11}, whereas the *m*-methoxy group approaches the side chains of M^{p47}.

apparent global minimum found by hands-free docking of such a flexible ligand as verapamil in a homology model of the channel with flexible side chains would be overoptimistic at least. On the other hand, ligand docking is the only currently available methodology that could be used as a substitute for extremely difficult and in most cases hardly doable crystallographic analyses of channel-ligand complexes. A solution for this dilemma is to use experimental data as constraints in energy calculations. It is noteworthy that a structure proposed by the constraints-driven docking should remain stable upon subsequent relaxation by Monte Carlo minimization (or molecular dynamics) without any constraints. Relaxation by simple energy minimization cannot be used to estimate the model stability because the energy landscape is extremely rugged, and constraints may cause the system to be trapped in a high-energy local minimum from which it is not possible to find an exit by simple energy minimization. The ligand-protein energy of the refined re-

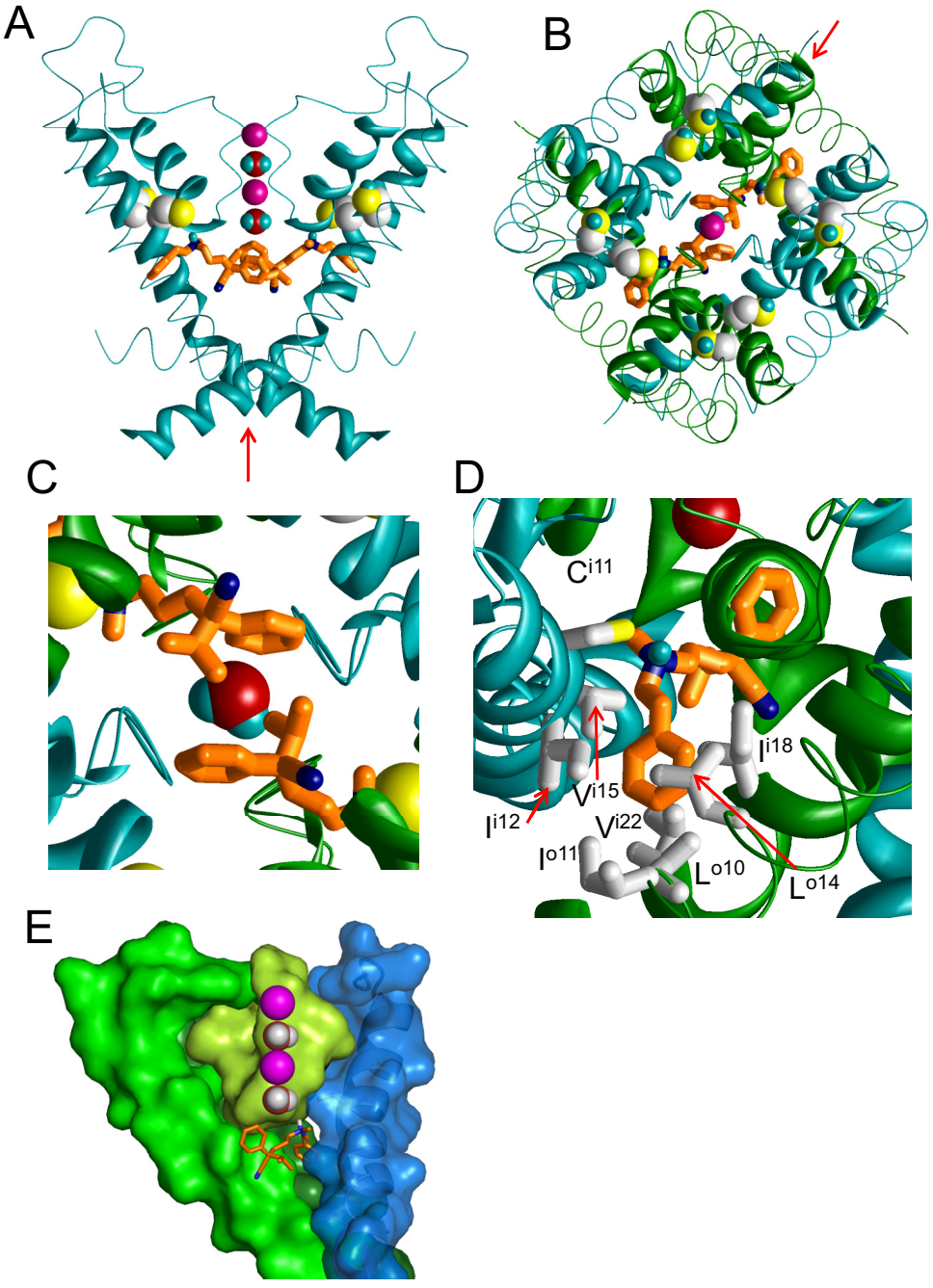

Fig. 8. Model of the Kv1.3 mutant $A^{i11}C$ with two emopamil molecules. The ligands' ammonium groups donate H-bonds to the sulfur atoms of C^{i11}, whereas the aromatic rings B hide in the hydrophobic intersubunit niches. Side chains of C^{i10} and C^{i11} are space-filled at A to C. A, side view with two subunits removed for clarity. B, Extracellular view in which two subunits are colored green and two subunits are cyan. C, close-up cytoplasmic view along the red arrow shown in A. Note close contacts between the aromatic and the isopropyl groups of the two ligands that would make the pore impermeable. D, view along the P-helix along the red arrow indicated in B. Side chains of the hydrophobic residues, which are located in the interface between subunits within 5 Å from ring B of the emopamil molecule, are shown by sticks. The aromatic ring of emopamil fits snugly in the hydrophobic interface, whereas the methoxylated ring of verapamil would experience sterical clashes and unfavorable dehydration. E, surface representation with the channel segments colored as in Fig. 7D. The intersubunit niche accommodates ring B of emopamil.

TABLE 2
Residues in the intersubunit niche of the Kv1.3 channel versus matching residues in the $Ca_v1.2$ channel

Channel	Residue						
Kv1.3	Leu^{o10}	Ile^{o11}	Leu^{o14}	Ile^{i18}	Val^{i22}	Ile^{i12}	Val^{i15}
$Ca_v1.2$	Ile^{3o10}	Val^{3o11}	Thr^{3o14}	Met^{3i18}	Phe^{3i22}	Met^{4i12}	Ala^{4i15}

laxed system should be negative, and furthermore, the partitioned energy contributions of all residues, which are in direct contact with the ligand, should also be negative to indicate the absence of sterical clashes. Whether the energy of the active complex predicted in a homology model (which is obviously less precise than a high-resolution X-ray structure) corresponds to the apparent global minimum is less important. However, if the predicted active complex corresponds to a local energy minimum, its energy should not be substantially higher (no more than 4 kcal/mol in our studies) than the energy of the apparent global minimum. It should be noted that models shown in Figs. 7 and 8 satisfy all of these criteria.

Results of our constraints-driven docking provide structural explanations for available data on action of phenylalkylamines in hKv1.3 and its mutants. Important characteristics of the predicted complexes are the binding of the ammonium group to a cationophilic site in the cavity, the proximity of ring B to the P-loop turn, and the extension of the bulky pentanenitrilephenyl moiety along the inner pore, toward the cytoplasm. We did not find any specific interactions of the cyano group with the channel, in agreement with the observations that the IC_{50} value for the steady-state block of hKv1.3_H^{p56}T by (±)-acyanoverapamil is similar to that of (±)-verapamil (Dreker and Grissmer, 2005).

Our results suggest that ring B of the phenylalkylamines binds in the intrasubunit niche of Kv1.3, whereas this niche in the A^{i11}C mutant is obstructed by the cysteine side chain. Only the demethoxylated phenyl ring B of emopamil can penetrate the intersubunit niche of the mutant. In a model of devapamil in the $Ca_v1.2$ channel intra- and interdomain interfaces constitute binding loci for rings A and B, respectively (Cheng et al., 2009). Why does ring B of devapamil bind between helices 3P and 4S6 in $Ca_v1.2$, but does not bind between respective helices in Kv1.3? There may be two possible reasons. First, in the $Ca_v1.2$ channel model, Y^{4i11} donates an H-bond to the *meta*-methoxy group in ring B of devapamil, whereas Kv1.3 contains A^{i11} in the respective position. Second, several bulky residues in the intersubunit niche of Kv1.3 (Fig. 8D) have less bulky analogs in the $Ca_v1.2$ channel (Table 2).

The inter- and intrasubunit niches can be seen in surface images of the channel with the ligands that extend their moieties to the niches (Figs. 7D and 8E). Whereas the intrasubunit niche (Fig. 7D) seems smaller than the intersubunit niche (Fig. 8E), the former can accommodate a part of ring B. The side chains of A^{i11} and M^{p47} do not occlude the entrance to the niche because the C^{α}–C^{β} bonds of these residues extend along the niche walls (Fig. 2, G and F). Bonds A^{i11}_C^{α}-C^{β} and M^{p47}_C^{α}–C^{β} direct toward the pore and away from it, respectively. The flexible side chain of M^{p47} can adopt conformations in which atoms S^{δ} and/or C^{ε} can approach the *meta*-methoxy group of verapamil to contribute to its binding pocket. This explains why the mutation M^{p47}V decreases Kv1.3-blocking potency of verapamil 6-fold (Rauer and Grissmer, 1999). The side chains of T^{p48} and T^{p49} do not contribute to verapamil binding in our models, in agreement with data that mutations T^{p48}S and T^{p49}A do not cause noticeable effects on Kv1.3 block by verapamil (Rauer and Grissmer, 1999).

The important and rather unexpected prediction of our calculations is the H-bonding of the ammonium group of emopamil to the sulfur atom of C^{i11}. Parameters for the N-H---S H-bonds are present in the earlier version of the AMBER force field that is implemented in the ZMM program. The ability of sulfur to accept H-bonds has been demonstrated from analysis Cambridge Structural Database (Allen et al., 1997). H-bonds N-H---S were found in crystals of small molecules (Chung et al., 1991). In the X-ray structure of *Mycobacterium tuberculosis,* LipB enzyme (Protein Data Bank code 1W66), the distance between the lysine side chain N and the cysteine S, is as small as 3.42 Å (Ma et al., 2006). The formation of strong N-H---S bonds was recently demonstrated experimentally and by high-level computations (Biswal and Wategaonkar, 2009). In conclusion, this study explains the intriguing peculiarities of structure-activity relationships of phenylalkylamines interacting with Kv1.3 channels and its A^{i11}C mutant, proposing atomistic details for the channel block by this important class of ligands.

Acknowledgments

We thank Daniel Garden for PYMOL images shown in Figs. 7D and 8E.

Authorship Contributions

Participated in research design: Rossokhin, Dreker, Grissmer, and Zhorov.

Conducted experiments: Rossokhin, Dreker, and Zhorov.

Performed data analysis: Rossokhin, Dreker, Grissmer, and Zhorov.

Wrote or contributed to the writing of the manuscript: Rossokhin, Dreker, Grissmer, and Zhorov.

Other: Grissmer and Zhorov acquired funding for the research.

References

Allen FH, Bird CM, Rowland RS and Raithby PR (1997) Hydrogen-bond acceptor and donor properties of divalent sulfur (Y-S-Z and R-S-H). *Acta Crystallogr* **53:**696–701.

Armstrong CM (1971) Interaction of tetraethylammonium ion derivatives with the potassium channels of giant axons. *J Gen Physiol* **58:**413–437.

Armstrong CM and Hille B (1972) The inner quaternary ammonium ion receptor in potassium channels of the node of Ranvier. *J Gen Physiol* **59:**388–400.

Biswal HS and Wategaonkar S (2009) Nature of the N-H. . .S hydrogen bond. *J Phys Chem A* **113:**12763–12773.

Bruhova I, Tikhonov DB, and Zhorov BS (2008) Access and binding of local anesthetics in the closed sodium channel. *Mol Pharmacol* **74:**1033–1045.

Bruhova I and Zhorov BS (2005) KvAP-based model of the pore region of shaker potassium channel is consistent with cadmium- and ligand-binding experiments. *Biophys J* **89:**1020–1029.

Chandy KG, DeCoursey TE, Cahalan MD, McLaughlin C, and Gupta S (1984) Voltage-gated potassium channels are required for human T lymphocyte activation. *J Exp Med* **160:**369–385.

Chandy KG, Wulff H, Beeton C, Pennington M, Gutman GA, and Cahalan MD (2004) K^+ channels as targets for specific immunomodulation. *Trends Pharmacol Sci* **25:**280–289.

Cheng RC, Tikhonov DB, and Zhorov BS. (2009) Structural model for phenylalkylamine binding to L-type calcium channels. *J Biol Chem* **284:**28332–28342.

Choi KL, Mossman C, Aubé J, and Yellen G (1993) The internal quaternary ammonium receptor site of Shaker potassium channels. *Neuron* **10:**533–541.

Chung WP, Dewan JC, and Walters MA (1991) Models of lysine-cysteine hydrogen bonding in metallothionein: hydrogen bonding between ammonium and benzenethiolate in $[(C_6H_{11})_2\ NH_2]_2[Co(SC_6H_5)_4]$. *J Am Chem Soc* **113:**525–530.

DeCoursey TE (1995) Mechanism of K^+ channel block by verapamil and related compounds in rat alveolar epithelial cells. *J Gen Physiol* **106:**745–779.

DeCoursey TE, Chandy KG, Gupta S, and Cahalan MD. (1984) Voltage-gated K^+ channels in human T lymphocytes: a role in mitogenesis? *Nature* **307:**465–468.

DeCoursey TE, Chandy KG, Gupta S, and Cahalan MD (1985) Voltage-dependent ion channels in T-lymphocytes. *J Neuroimmunol* **10:**71–95.

Dewar MJ, Zoebisch EG, Healy EF, and Stewart JJ (1985) AM1: A new general purpose quantum mechanical molecular model. *J Am Chem Soc* **107:**3902–3909.

Doyle DA, Morais Cabral J, Pfuetzner RA, Kuo A, Gulbis JM, Cohen SL, Chait BT, and MacKinnon R (1998) The structure of the potassium channel: molecular basis of K^+ conduction and selectivity. *Science* **280:**69–77.

Dreker T and Grissmer S (2005) Investigation of the phenylalkylamine binding site in hKv1.3 (H399T), a mutant with a reduced C-type inactivated state. *Mol Pharmacol* **68:**966–973.

Garden DP and Zhorov BS (2010) Docking flexible ligands in proteins with a solvent exposure- and distance-dependent dielectric function. *J Comput Aided Mol Des* **24:**91–105.
Hamill OP, Marty A, Neher E, Sakmann B, and Sigworth FJ (1981) Improved patch-clamp techniques for high-resolution current recording from cells and cell-free membrane patches. *Pflugers Arch* **391:**85–100.
Hille B (2001) *Ionic Channels of Excitable Membrane*, Sinauer Associates, Inc., Sunderland, MA.
Jacobs ER and DeCoursey TE (1990) Mechanisms of potassium channel block in rat alveolar epithelial cells. *J Pharmacol Exp Ther* **255:**459–472.
Jiang Y, Lee A, Chen J, Cadene M, Chait BT, and MacKinnon R. (2002) Crystal structure and mechanism of a calcium-gated potassium channel. *Nature* **417:**515–522.
Jiang Y, Lee A, Chen J, Ruta V, Cadene M, Chait BT, and MacKinnon R (2003) X-ray structure of a voltage-dependent K^+ channel. *Nature* **423:**33–41.
Kostyuk PG, Krishtal OA, and Doroshenko PA (1975) Outward currents in isolated snail neurons. III. Effect of verapamil. *Comp Biochem Physiol C* **51:**269–274.
Lazaridis T and Karplus M (1999) Effective energy function for proteins in solution. *Proteins* **35:**133–152.
Li Z and Scheraga HA (1987) Monte Carlo-minimization approach to the multiple-minima problem in protein folding. *Proc Natl Acad Sci USA* **84:**6611–6615.
Long SB, Campbell EB, and Mackinnon R (2005) Crystal structure of a mammalian voltage-dependent Shaker family K^+ channel. *Science* **309:**897–903.
Ma Q, Zhao X, Nasser Eddine A, Geerlof A, Li X, Cronan JE, Kaufmann SH, and Wilmanns M (2006) The *Mycobacterium tuberculosis* LipB enzyme functions as a cysteine/lysine dyad acyltransferase. *Proc Natl Acad Sci USA* **103:**8662–8667.
Momany FA, McGuire RF, Burgess AW, and Scheraga HA (1975) Energy parameters in polypeptides. VII. Geometric parameters, partial atomic charges, nonbonded interactions, hydrogen bond interactions, and intrinsic torsional potentials of the naturally occurring amino acids. *J Phys Chem* **79:**2361–2381.
Morais-Cabral JH, Zhou Y, and MacKinnon R (2001) Energetic optimization of ion conduction rate by the K^+ selectivity filter. *Nature* **414:**37–42.
Nagano N, Ota M, and Nishikawa K (1999) Strong hydrophobic nature of cysteine residues in proteins. *FEBS Lett* **458:**69–71.
Pelzer D, Trautwein W, and McDonald TF (1982) Calcium channel block and recovery from block in mammalian ventricular muscle treated with organic channel inhibitors. *Pflugers Arch* **394:**97–105.
Rauer H and Grissmer S (1996) Evidence for an internal phenylalkylamine action on the voltage-gated potassium channel Kv1.3. *Mol Pharmacol* **50:**1625–1634.
Rauer H and Grissmer S (1999) The effect of deep pore mutations on the action of phenylalkylamines on the Kv1.3 potassium channel. *Br J Pharmacol* **127:**1065–1074.
Retzinger GS, Cohen L, Lau SH, and Kézdy FJ (1986) Ionization and surface properties of verapamil and several verapamil analogues. *J Pharm Sci* **75:**976–982.
Rossokhin A, Teodorescu G, Grissmer S, and Zhorov BS (2006) Interaction of d-tubocurarine with potassium channels: molecular modeling and ligand binding. *Mol Pharmacol* **69:**1356–1365.
Strutz-Seebohm N, Gutcher I, Decher N, Steinmeyer K, Lang F, and Seebohm G (2007) Comparison of potent Kv1.5 potassium channel inhibitors reveals the molecular basis for blocking kinetics and binding mode. *Cell Physiol Biochem* **20:**791–800.
Tamargo J, Caballero R, Gómez R, Valenzuela C, and Delpón E (2004) Pharmacology of cardiac potassium channels. *Cardiovasc Res* **62:**9–33.
Tikhonov DB, Bruhova I, and Zhorov BS (2006) Atomic determinants of state-dependent block of sodium channels by charged local anesthetics and benzocaine. *FEBS letters* **580:**6027–6032.
Tikhonov DB and Zhorov BS (2008) Molecular modeling of benzothiazepine binding in the L-type calcium channel. *J Biol Chem* **283:**17594–17604.
Weiner J, Kollman PA, Case DA, Singh UC, Chio C, Alagona G, Profeta S, and Weiner PK (1984) A new force field for molecular mechanical simulation of nucleic acids and proteins. *J Am Chem Soc* **106:**765–784.
Weiner SJ, Kollman PA, Nguyen DT, and Case DA (1986) An all atom force field for simulations of proteins and nucleic acids. *J Comput Chem* **7:**230–252.
Wit AL and Cranefield PF (1974) Effect of verapamil on the sinoatrial and atrioventricular nodes of the rabbit and the mechanism by which it arrests reentrant atrioventricular nodal tachycardia. *Circ Res* **35:**413–425.
Wulff H and Zhorov BS (2008) K^+ channel modulators for the treatment of neurological disorders and autoimmune diseases. *Chem Rev* **108:**1744–1773.
Zhang RM and Snyder GH (1989) Dependence of formation of small disulfide loops in two-cysteine peptides on the number and types of intervening amino acids. *J Biol Chem* **264:**18472–18479.
Zhang S, Zhou Z, Gong Q, Makielski JC, and January CT (1999) Mechanism of block and identification of the verapamil binding domain to HERG potassium channels. *Circ Res* **84:**989–998.
Zhorov BS (1981) Vector method for calculating derivatives of energy of atom-atom interactions of complex molecules according to generalized coordinates. *J Struct Chem* **22:**4–8.
Zhorov BS and Tikhonov DB (2004) Potassium, sodium, calcium and glutamate-gated channels: pore architecture and ligand action. *J Neurochem* **88:**782–799.
Zhou M, Morais-Cabral JH, Mann S, and MacKinnon R (2001b) Potassium channel receptor site for the inactivation gate and quaternary amine inhibitors. *Nature* **411:**657–661.
Zhou Y and MacKinnon R (2003) The occupancy of ions in the K^+ selectivity filter: charge balance and coupling of ion binding to a protein conformational changes underlie high conduction rate. *J Mol Biol* **333:**965–975.
Zhou Y, Morais-Cabral JH, Kaufman A, and MacKinnon R (2001a) Chemistry of ion coordination and hydration revealed by a K^+ channel-Fab complex at 2.0 A resolution. *Nature* **414:**43–48.

Address correspondence to: Dr. Boris S. Zhorov, Department of Biochemistry and Biomedical Sciences, McMaster University, Hamilton, ON, Canada. E-mail: zhorov@mcmaster.ca